Title: Targeting CD46 for both adenocarcinoma and neuroendocrine prostate cancer

Authors: Yang Su, Yue Liu, Christopher R. Behrens, Scott Bidlingmaier, Nam-Kyung Lee, Rahul Aggarwal, Daniel W. Sherbenou, Alma L. Burlingame, Byron C. Hann, Jeffry P. Simko, Gayatri Premasekharan, Pamela L. Paris, Marc A. Shuman, Youngho Seo, Eric J. Small, and Bin Liu

Supplementary materials

Materials and methods

Supplemental Table S1: Gene expression of CD46 and PSMA (FOLH1) in adenocarcinoma and neuroendocrine CRPC.

Supplemental Table S2: Clinical characteristics of prostate patients in the CTC study.

Supplemental Figure S1: Identification of the target antigen as CD46.

Supplemental Figure S2: Tumor cell specific binding and cytotoxicity.

Supplemental Figure S3: Close-up views of CD46 IHC staining in prostate cancer FFPE tissues.

Supplemental Figure S4: Close-up views of CD46 IHC staining in normal human FFPE tissues.

Supplemental Figure S5: Characterization of a panel of newly identified anti-CD46 human monoclonal antibodies.

Supplemental Figure S6: Close-up views of CD46 IHC staining in normal human frozen tissues: placenta, prostate, kidney, and liver.

Supplemental Figure S7: Close-up views of CD46 IHC staining in normal human frozen tissues: stomach, heart, colon, and smooth muscle.

Supplemental Figure S8: Close-up views of CD46 IHC staining in normal human frozen tissues: cerebellum, peripheral nerve, lymph node, small intestine, and lung.

Supplemental Figure S9: H protein internalization by prostate cancer cells via macropinocytosis.

Supplemental Figure S10: Anti-CD46 human antibodies are internalized by macropinocytosis by mCRPC cell lines.

Supplemental Figure S11: Subcellular localization of macropinocytosed anti-CD46 YS5 IgG1 in mCRPC cell lines.

Supplemental Figure S12: Lack of macropinocytosis and anti-CD46 antibody uptake by normal T cells.

Supplemental Figure S13: Characterization of anti-CD46 ADC.

Supplemental Figure S14: Body weight assessment in *in vivo* intra-femoral bone tumor xenograft model.

Supplemental Figure S15: CD46 expression in neuroendocrine mCRPC cell and tissue.

Supplemental Figure S16: Close-up views of CD46 IHC staining (shown in Figure S15C) in neuroendocrine type mCRPC.

Supplemental Figure S17: CD46 internalization via macropinocytosis by neuroendocrine prostate cancer cell line H660.

Supplemental Figure S18: Subcellular localization of anti-CD46 antibody post internalization into neuroendocrine prostate cancer cells.

Supplemental Figure S19: CD46 upregulation following ASI treatment.

Supplemental Figure S20: Exploratory tox study in non-human primates.

Supplemental Figure S21: Blood chemistry change in exploratory tox study.

Supplemental Table 1. Gene expression of CD46 and PSMA (FOLH1) in adenocarcinoma (Adeno) and neuroendocrine (NE) CRPC. #CRPC-NE: the number of neuroendocrine CRPC cases. #CRPC-Adeno: the number of adenocarcinoma CRPC cases.

Gene	CRPC-Adeno mean expression	CRPC-NE mean expression	#CRPC-NE	#CRPC-Adeno
CD46	4.97	4.29	43	53
FOLH-1	4.5	1.42	43	53

Supplemental Table 2. Clinical characteristics of prostate patients in the CTC study. Abi: abiraterone. Enza: enzalutamide.

Patient #	Age (yrs)	Disease or PSA status	Abi or Enza resistance
1	63	Stable disease	Naive
2	75	PSA rising	Abi resistance
3	67	PSA rising	Naive
4	74	PSA rising	Enza resistance
5	72	PSA rising	Enza resistance
6	86	PSA rising	Naive

Supplemental Figure S1: Identification of the target antigen as CD46. The prostate cancer cell line DU145 was biotin-labeled to tag cell surface proteins. Cell lysates were incubated with UA20 scFv-Fc crosslinked to protein A beads, and the immunoprecipitation product was split into two portions, with one analyzed by SDS-PAGE followed by silver staining (A) and the other Western blot using streptavidin-HRP (B). Two bands with molecular weight between 55 – 72 kDa were identified in both (A) and (B) and were excised for mass spectrometry analysis. Both were identified as human CD46. Panel (C) shows molecular organization of human CD46. UA20 binds to a conformational epitope formed by Sushi domains 1 and 2, partially overlapping with the measles virus but not complement binding site. STP: serine threonine proline-rich region.

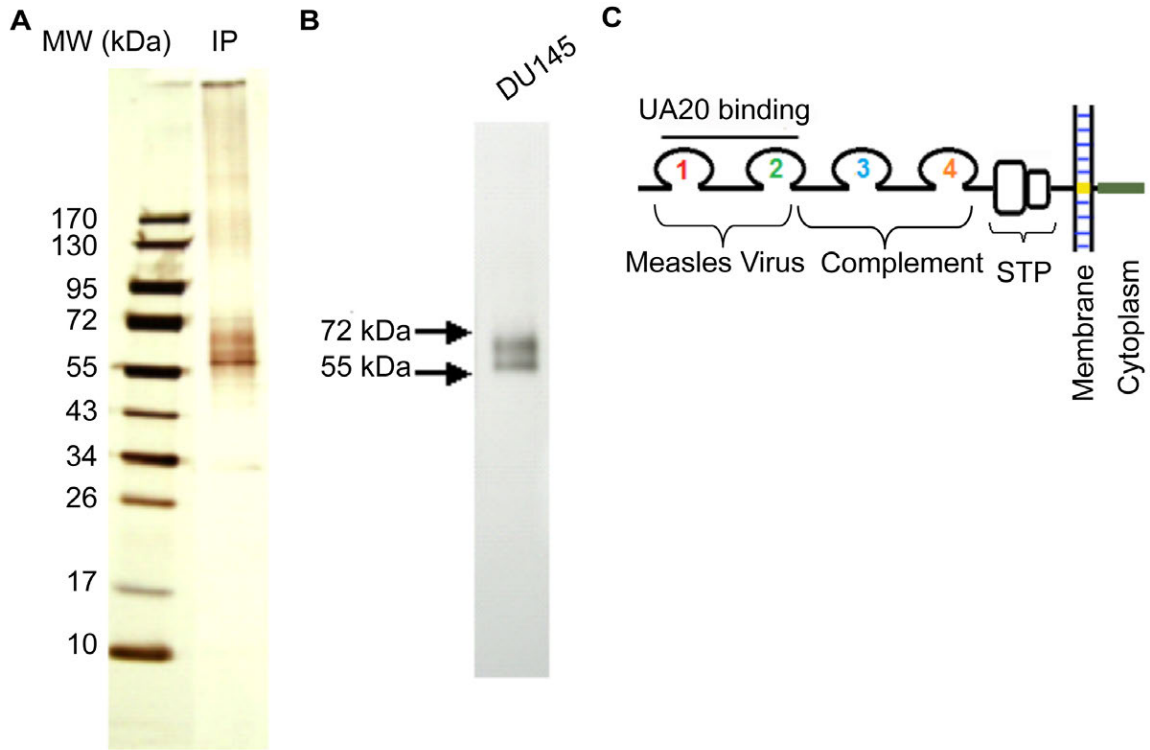

Supplemental Figure S2: Tumor cell specific binding and cytotoxicity. (A) The anti-CD46 antibody UA20 was analyzed by FACS for binding to the mCRPC line LNCaP-C4-2B and two control cell normal cell lines BPH-1 (a benign prostatic hyperplasia line) and HS775Li (a primary human liver cell line). Strong binding to LNCaP-C4-2B was observed with no or minimal binding to BPH-1 or HS775Li. Blue line, control; red line, UA20. (B) UA20 immunotoxin killed specifically the mCRPC line LNCaP-C4-2B (EC_{50} = 170 ± 36 pM) but not the control BPH-1 and HS775Li cells.

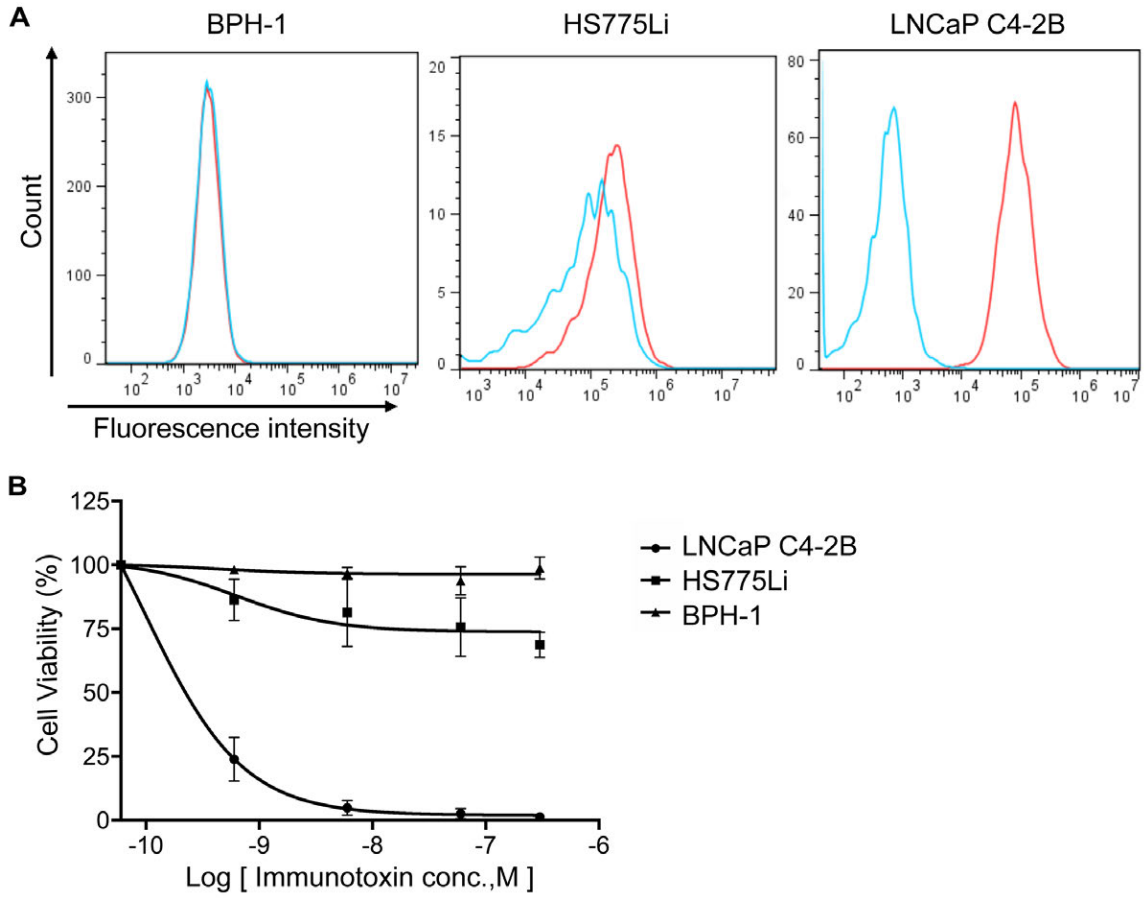

Supplemental Figure S3: Close-up views of CD46 IHC staining in prostate cancer FFPE tissues. CD46 protein is detected by affinity-purified rabbit polyclonal antibody H294. Scale bar: 150 μm for the left panel, and 30 μm for the right panel (close-up view). Low magnification images in the left panel are from Figure 1D, and reshown here to provide the tissue context of high magnification images in the right panel.

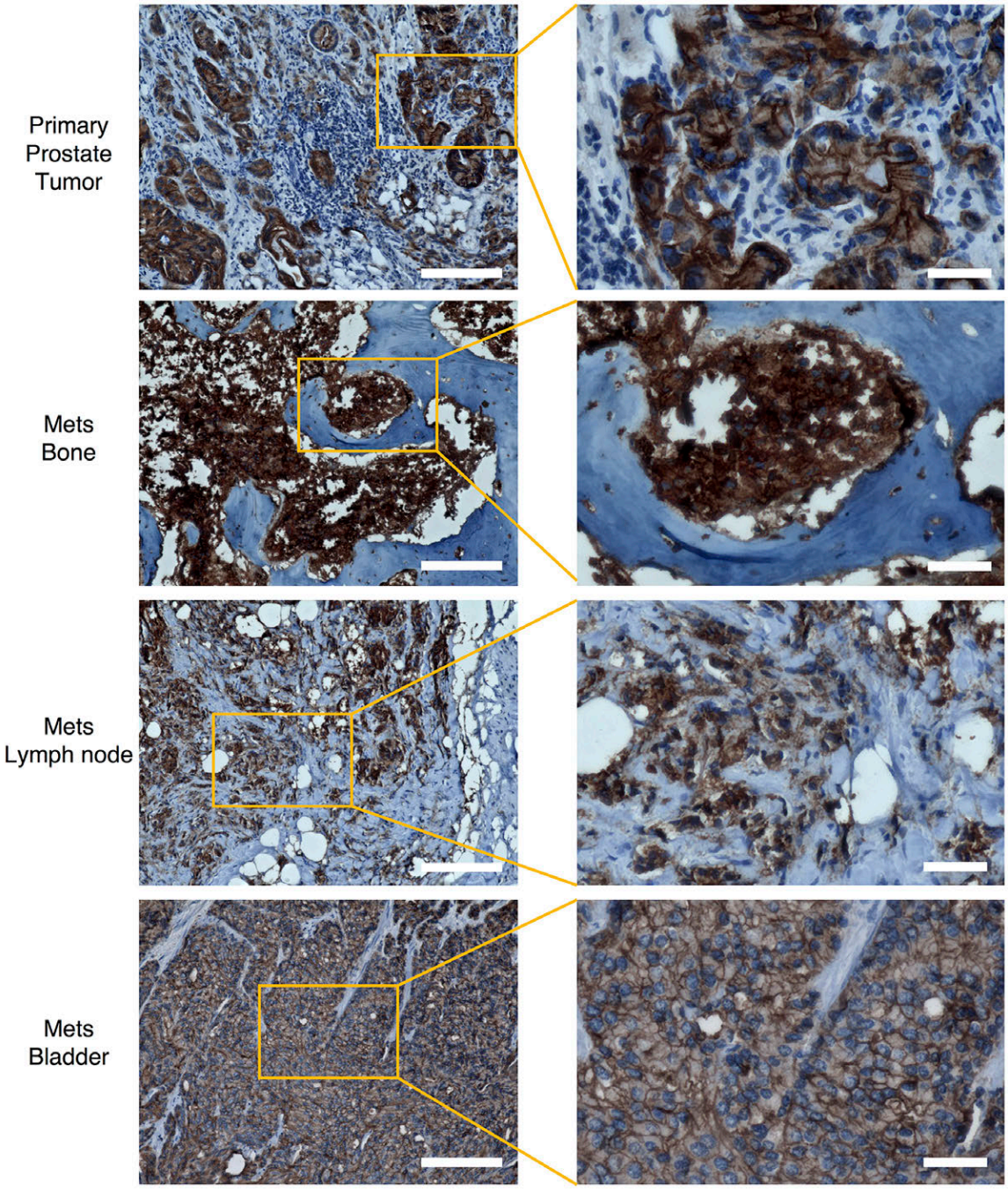

Supplemental Figure S4: Close-up views of CD46 IHC staining in normal human FFPE tissues. CD46 protein is detected by affinity-purified rabbit polyclonal antibody H294. Scale bar: 150 μm for the left panel, and 30 μm for the right panel (close-up view). Low magnification images in the left panel are from Figure 2C, and reshown here to provide the tissue context of high magnification images in the right panel.

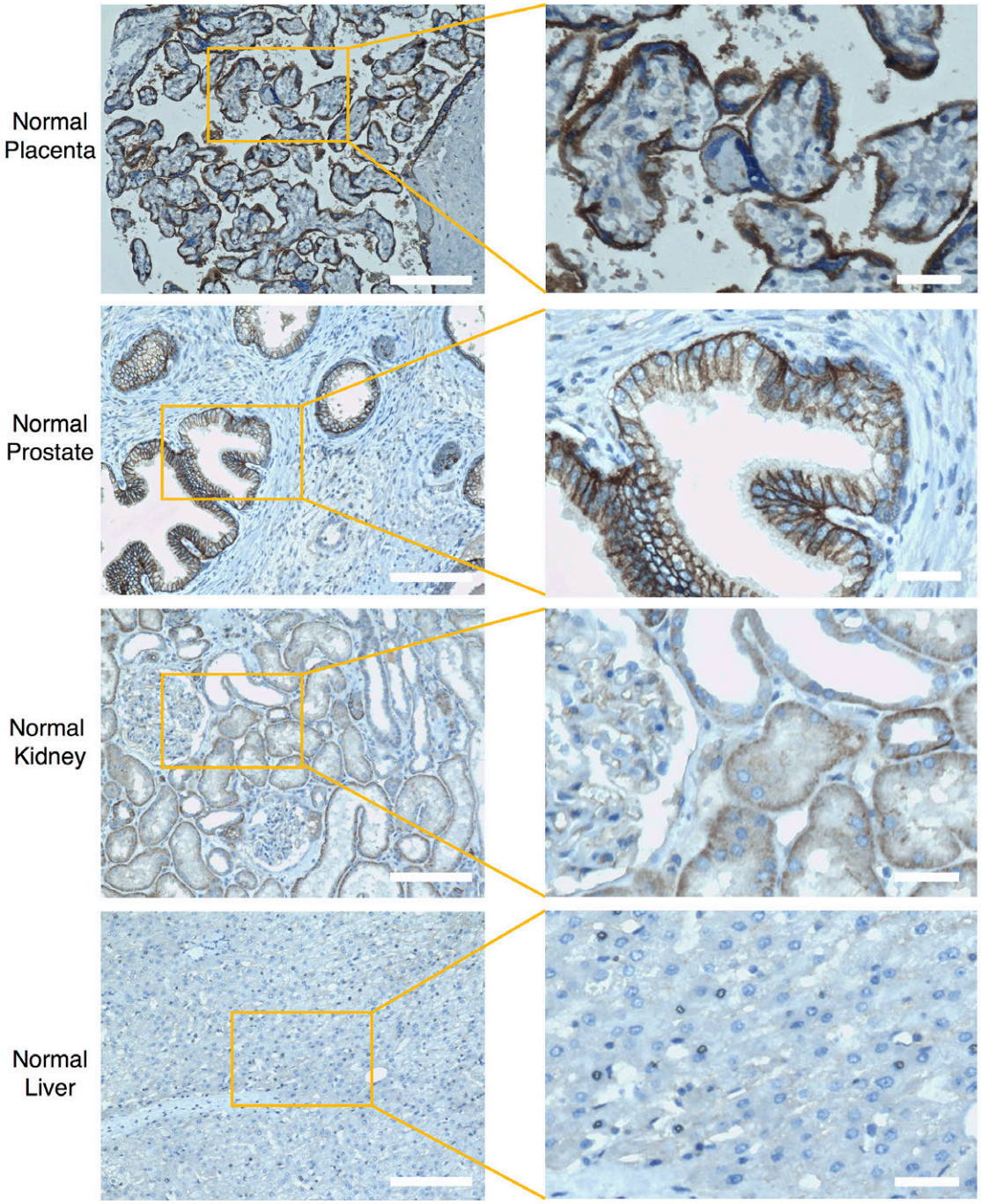

Supplemental Figure S5: Characterization of a panel of newly identified anti-CD46 human monoclonal antibodies. (A) Analysis of epitope overlap by competition with UA20. All but HGNY binds to an overlapping epitope with UA20. **** $p < 0.0001$. One-Way ANOVA, Bonferroni's multiple comparisons test. (B) No overlap with complement binding sites. Competitive C3b cell binding FACS was performed. None of the anti-CD46 antibodies blocked C3b binding to Du145 cells. One-Way ANOVA, Bonferroni's multiple comparisons test. (C) Partial overlap with oncolytic measles virus binding site. Competition FACS was performed to assess if any of the anti-CD46 antibodies blocks the binding of biotin-labeled measles virus H protein to DU145 cells. ** $p < 0.01$ ($p = 0.0087$), **** $p < 0.0001$, triplicates. One-Way ANOVA, Bonferroni's multiple comparisons test.

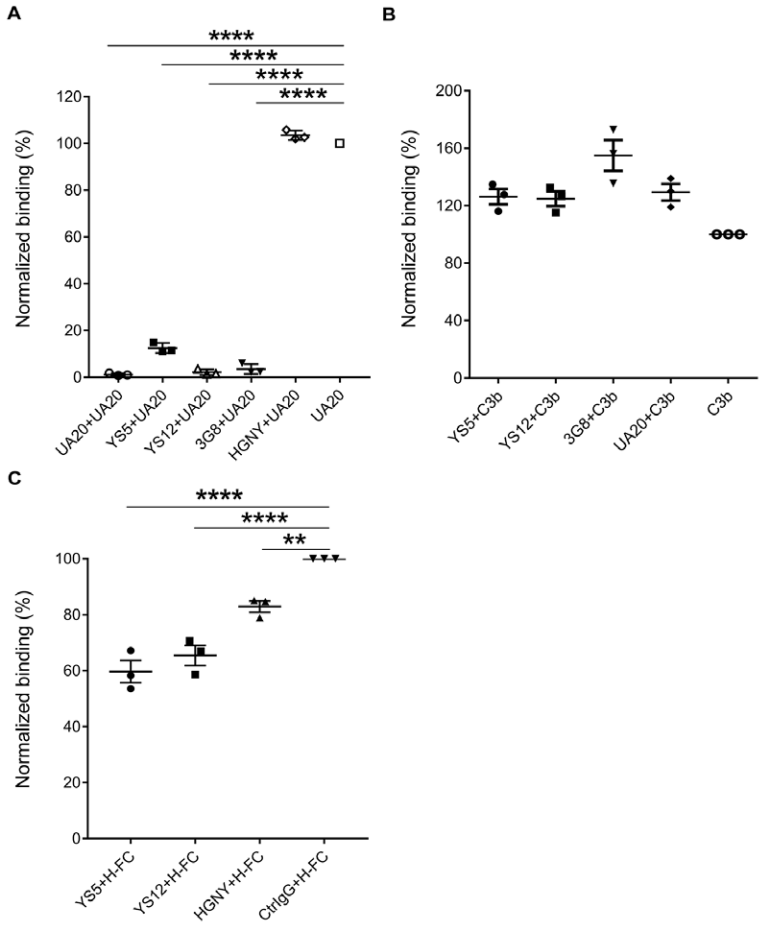

Supplemental Figure S6: Close-up views of CD46 IHC staining in normal human frozen tissues: placenta, prostate, kidney, and liver. The native CD46 epitope is detected by biotin-labeled human YS5 monoclonal antibody on a frozen human tissue array. Scale bar: 150 μm for the left panel, and 30 μm for the right panel (close-up view). Other than the normal placenta, low magnification images in the left panel are from Figure 2C, and reshown here to provide the tissue context of high magnification images in the right panel.

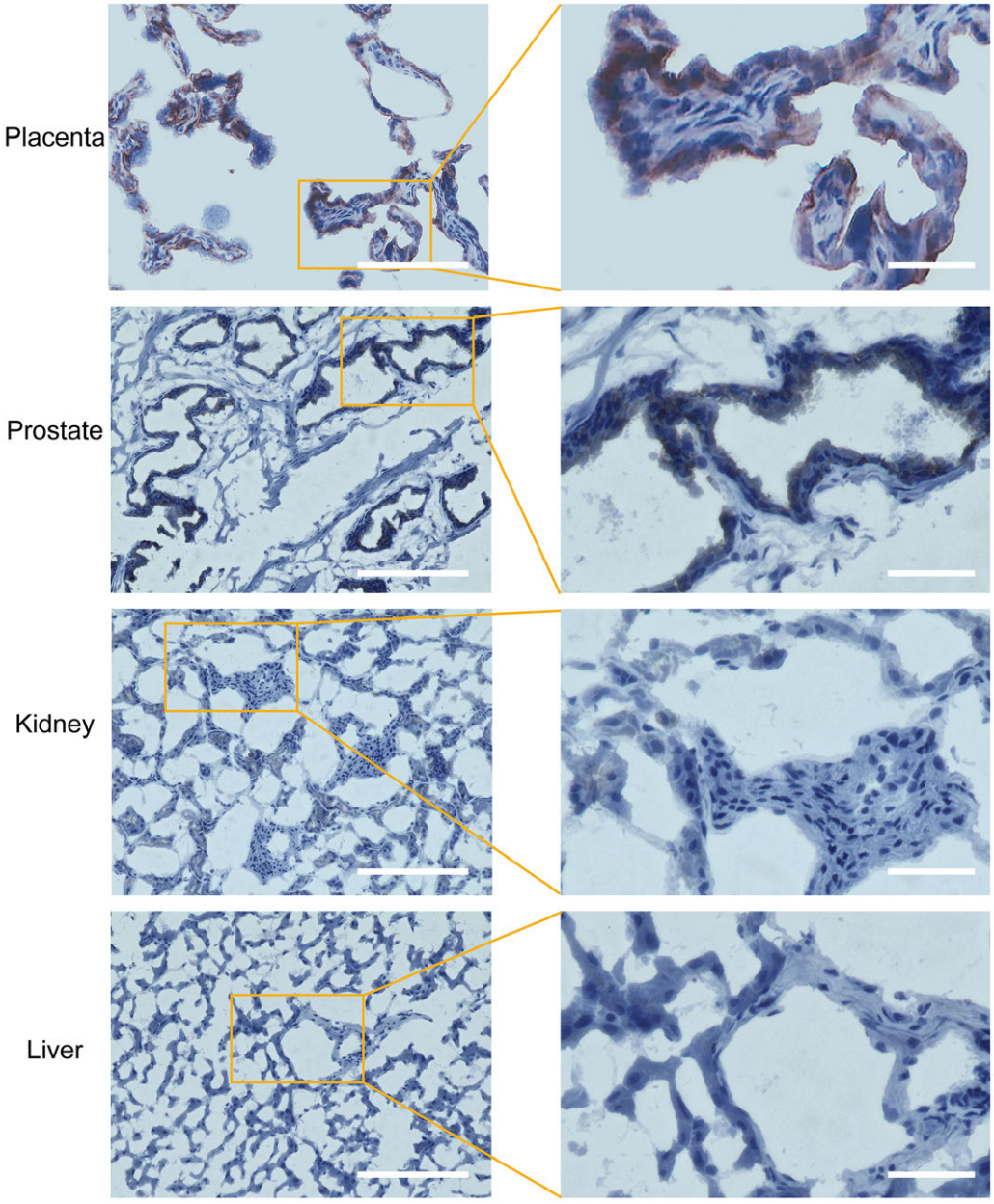

Supplemental Figure S7: Close-up views of CD46 IHC staining in normal human frozen tissues: stomach, heart, colon, and smooth muscle. The native CD46 epitope is detected by biotin-labeled human YS5 monoclonal antibody on a frozen human tissue array. Scale bar: 150 μm for the left panel, and 30 μm for the right panel (close-up view). Low magnification images in the left panel are from Figure 2C, and reshown here to provide the tissue context of high magnification images in the right panel.

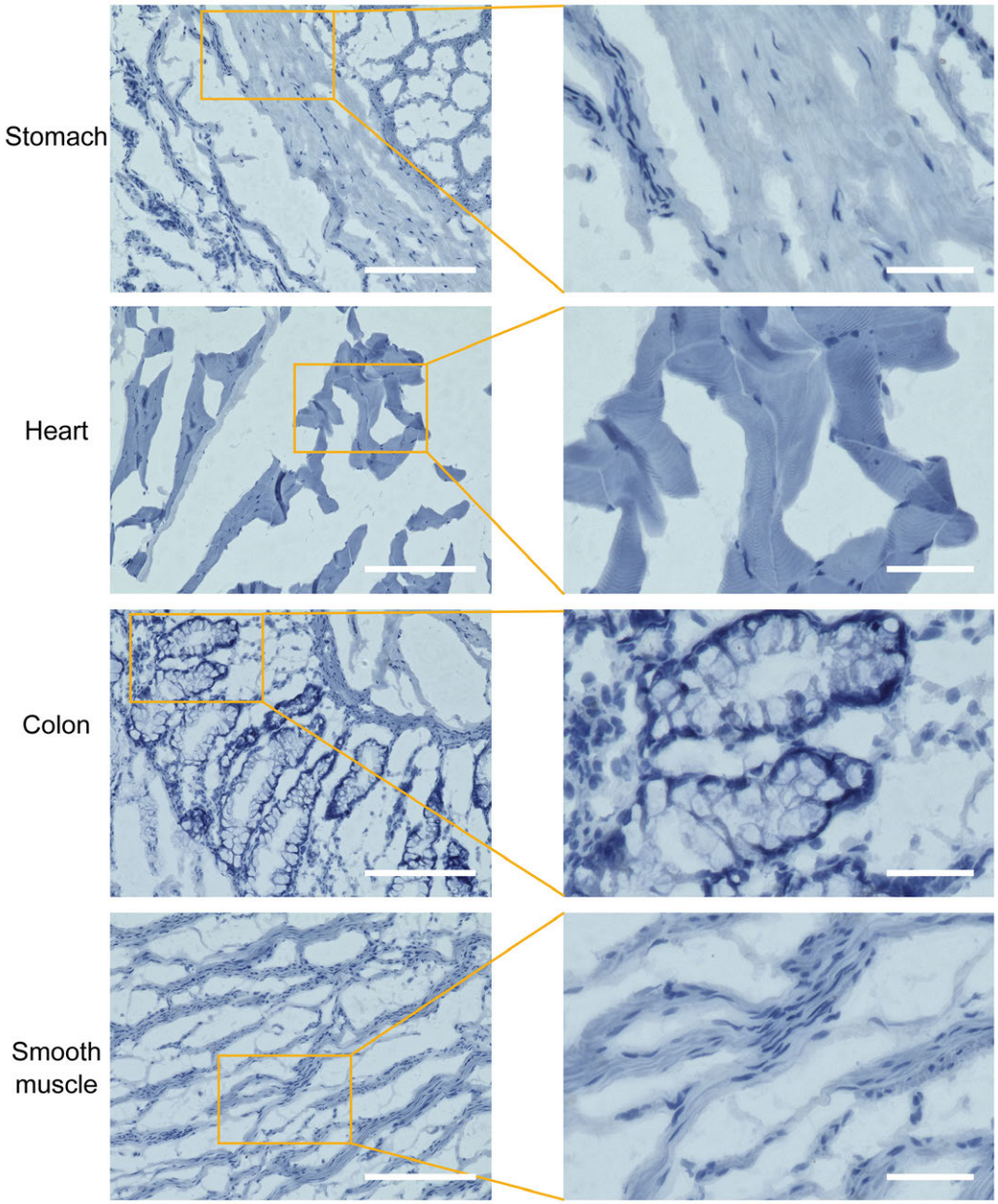

Supplemental Figure S8: Close-up views of CD46 IHC staining in normal human frozen tissues: cerebellum, peripheral nerve, lymph node, small intestine, and lung. The native CD46 epitope is detected by biotin-labeled human YS5 monoclonal antibody on a frozen human tissue array. Scale bar: 150 μm for the left panel, and 30 μm for the right panel (close-up view). Low magnification images in the left panel are from Figure 2C, and reshown here to provide the tissue context of high magnification images in the right panel.

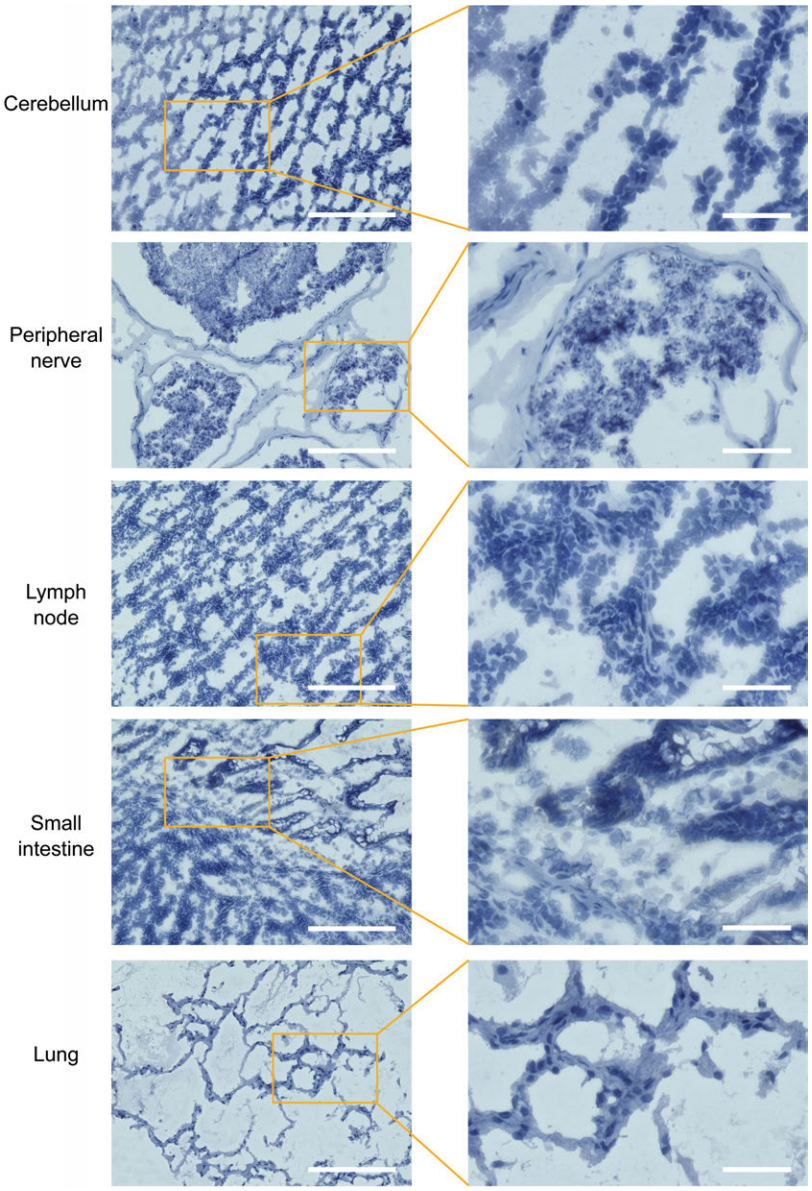

Supplemental Figure S9: H protein internalization by prostate cancer cells via macropinocytosis. Co-localization of the macropinocytosis marker ND70 and H protein (H-Fc) was studied by confocal microscopy. The rate of co-localization, calculated as the percent of double positive intracellular spots over antibody-positive intracellular spots, is 97.14% (34/35). Nuc: nucleus. Scale bar: 30 μm.

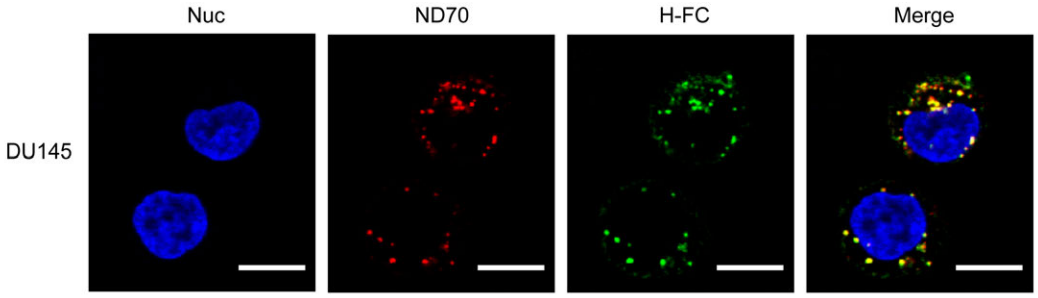

Supplemental Figure S10: Anti-CD46 human antibodies are internalized by macropinocytosis by a panel of mCRPC cell lines (DU145, LNCaP-C4-2B and PC3M). Co-localization of the macropinocytosis marker ND70 and YS5 IgG1 was studied by confocal microscopy. The rate of co-localization is 95.04% (134/141) for DU145, 80% (20/25) for LNCaP-C4-2B, and 98.59% (70/71) for PC3M. Anti-CD46 antibodies were incubated with mCRPC cell lines for 24 h before analysis. Nuc: nucleus. Scale bar: 30 µm.

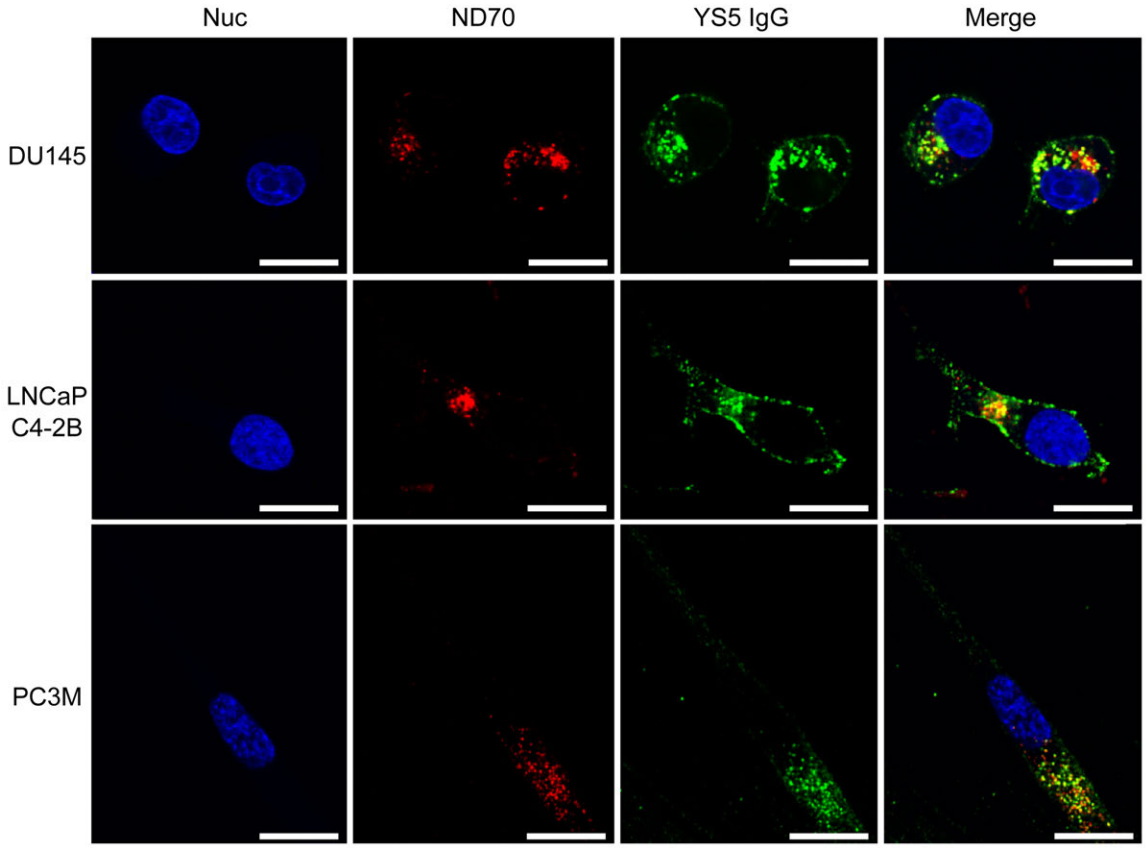

Supplemental Figure S11: Subcellular localization of macropinocytosed anti-CD46 YS5 IgG1 in mCRPC cell lines (DU145, LNCaP-C4-2B and PC3M). Confocal microscopy study was performed to determine YS5 co localization with lysosomes marked by LAMP1. The rate of co-localization is 81.48% (22/27) for DU145 and 96.55% (28/29) for LNCaP-C4-2B. For PC3M, the spots are clustered too closely to count, but the co-localization is evident. Nuc: nucleus. Scale bar: 30 μm.

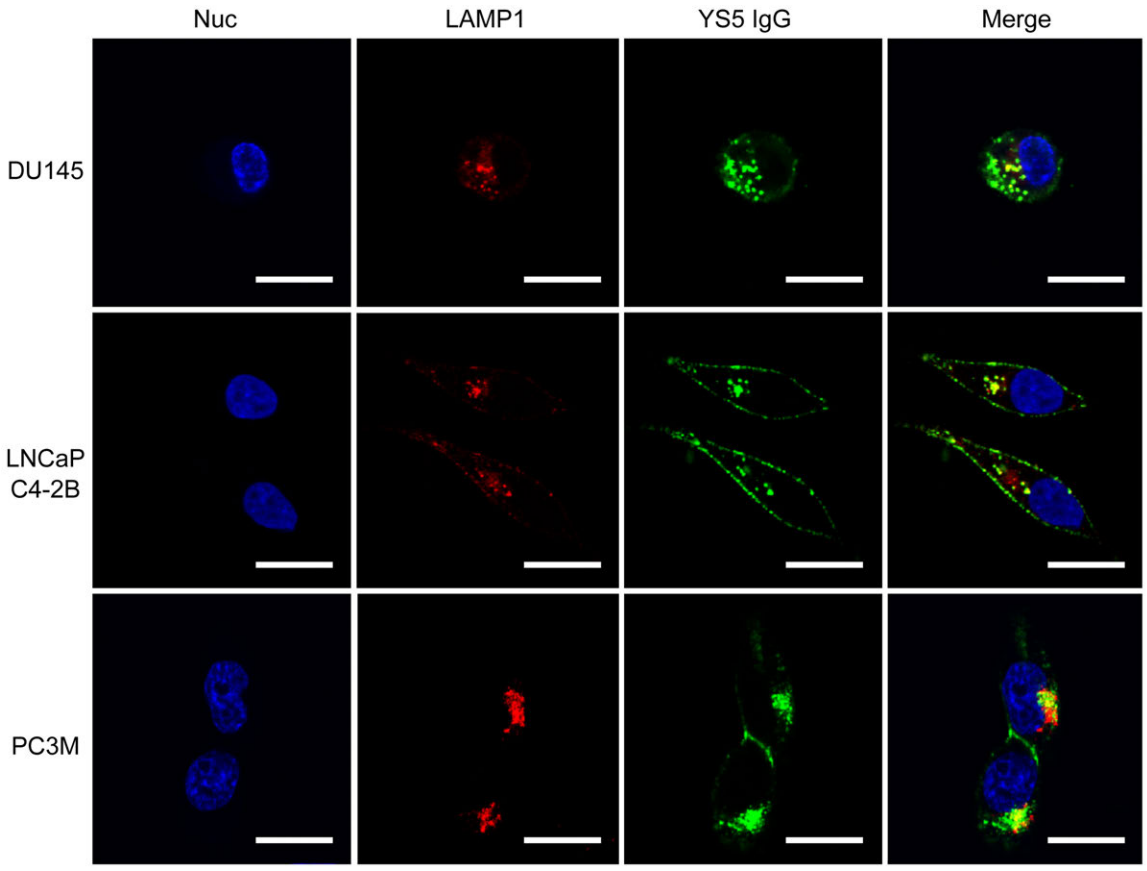

Supplemental Figure S12: Confocal analysis showed a lack of macropinocytosis and anti-CD46 antibody uptake by normal T cells. (A) No ND70 uptake by normal T cells after 24 h incubation. There was no YS5 IgG uptake during the same period. (B) Further analysis based on LAMP1 co-localization showed that there is no YS5 uptake and no colocalization with LAMP1 after either 4 h or 24 h incubation. Scale bar: 30 μm.

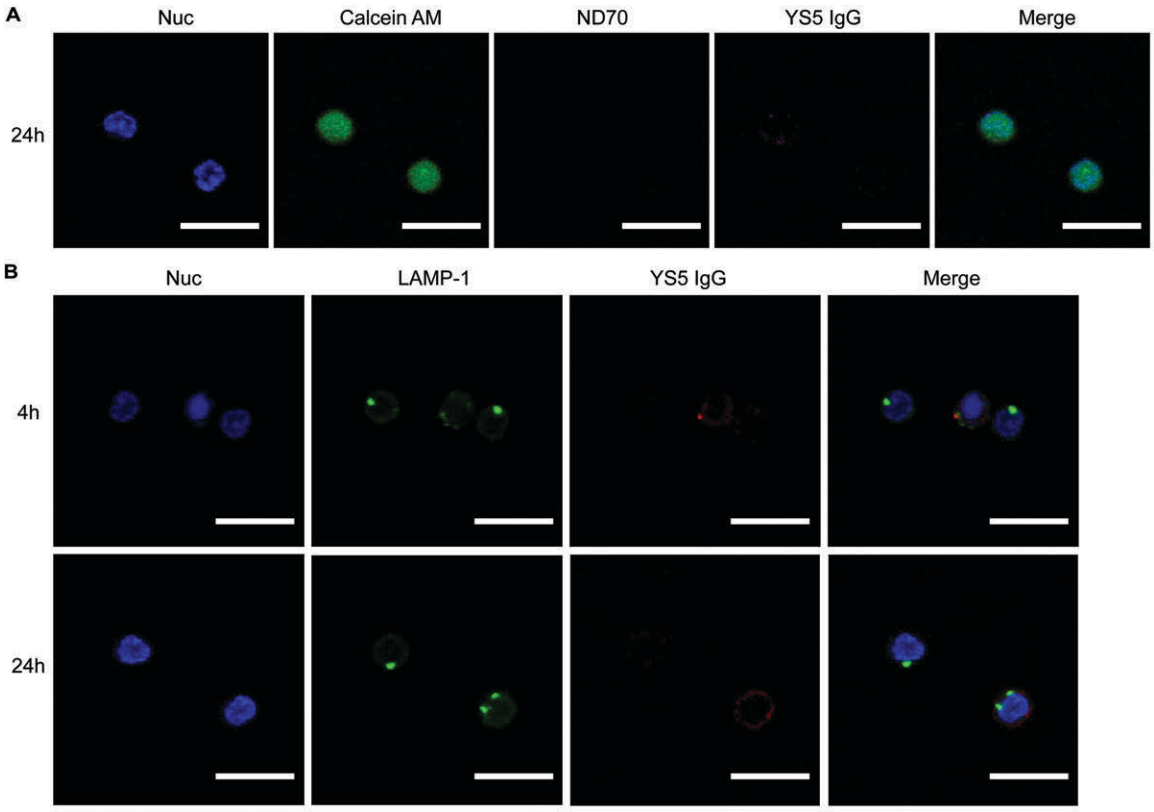

Supplemental Figure S13: Characterization of anti-CD46 ADC. (A) HPLC analysis. MMAF-conjugated YS5 IgG1 (YS5-MC-vc-PAB-MMAF) was analyzed on HIC column. Peaks corresponding to drug-to-antibody ratio (DAR) = 0, 2, 4, 6 and 8 are indicated. The control ADC (Ctrl IgG-MC-vc-PAB-MMAF) was analyzed the same way. (B) Assessment of cell binding. YS5 IgG1 and YS5 ADC (YS5-MC-vc-PAB-MMAF) showed similar binding to DU145 cells, suggesting minimal impact of drug conjugation on antibody-target interaction.

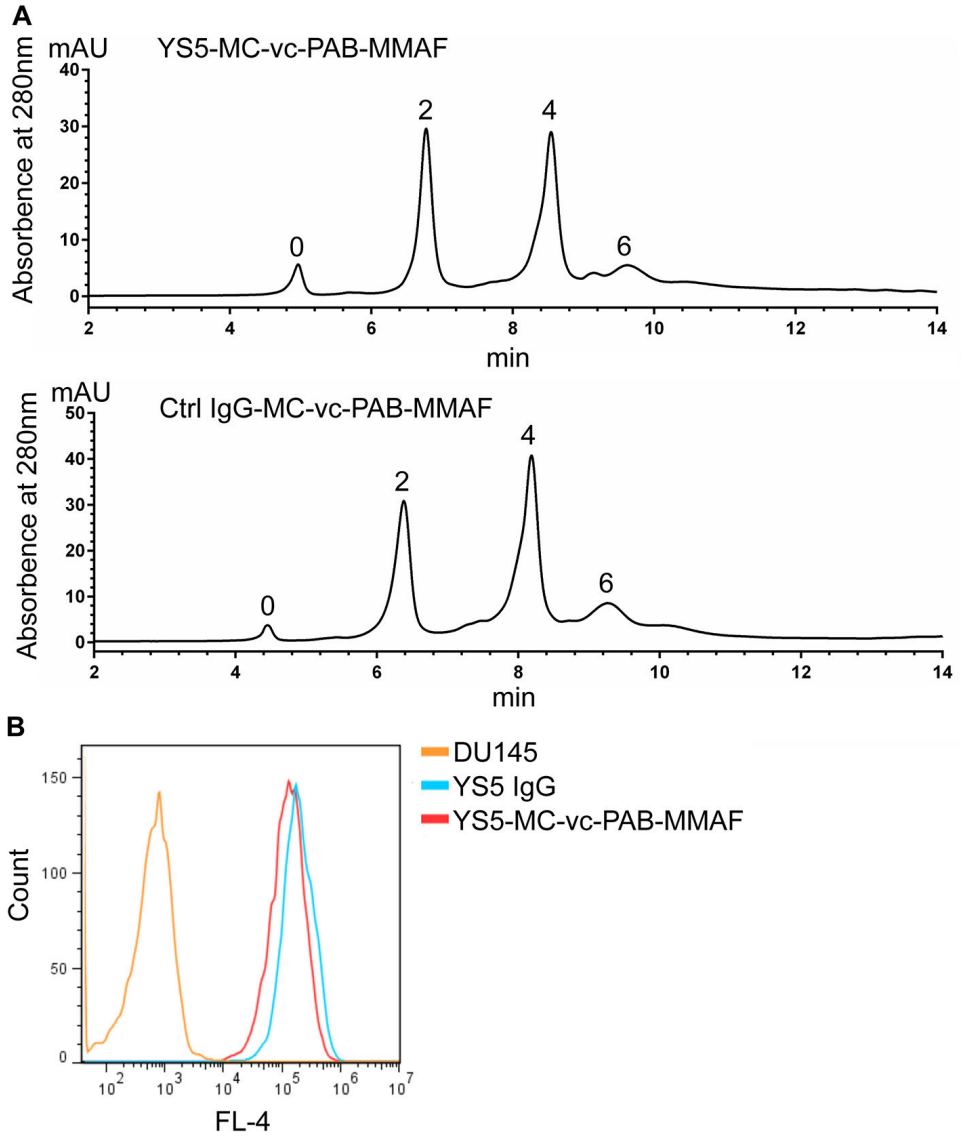

Supplemental Figure S14: Body weight change during the course of the intra-femoral xenograft study. CD46 ADC: YS5-MC-vc-pab-MMAF. Control ADC: Ctrl-MC-vc-pab-MMAF.

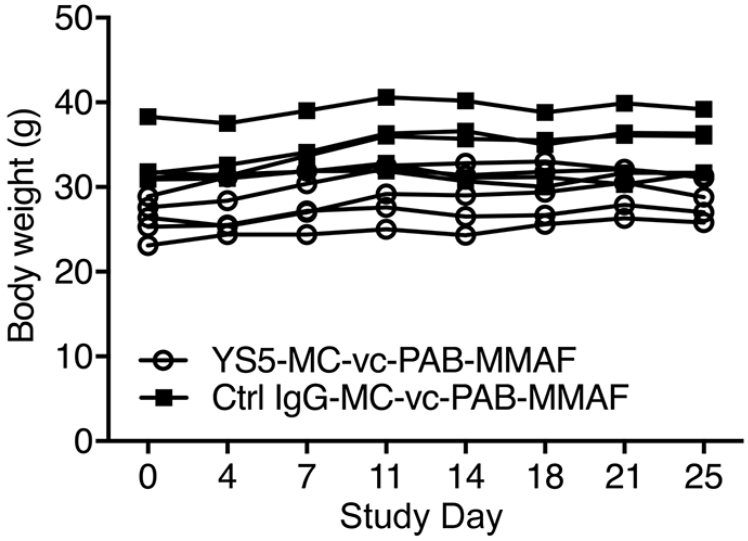

Supplemental Figure S15: CD46 expression in neuroendocrine-like mCRPC cells and neuroendocrine type of mCRPC tissues. (A) CD46 antigen density (surface copy number per cell) increased from 227,792 ± 22,396 to 501,262 ± 89,112 when LNCaP-C4-2B cells were co-incubated with CM from bone morrow stromal cell line HS5. SF: serum free. CM: conditioned media. Student's t test, unpaired two-tailed, triplicates. * $p < 0.05$ ($p = 0.0409$). (B) Induction of neuroendocrine-like phenotype. LNCaP-C4-2B co-cultured with HS5 CM but not control serum free media showed expression of the neuroendocrine marker NSE by Western blot analysis. (C) IHC analysis of mCRPC tissue specimen that underwent treatment-induced neuroendocrine differentiation. Co-expression of CD46 and NSE by prostate cancer cells was observed. Scale bar: 200 μm.

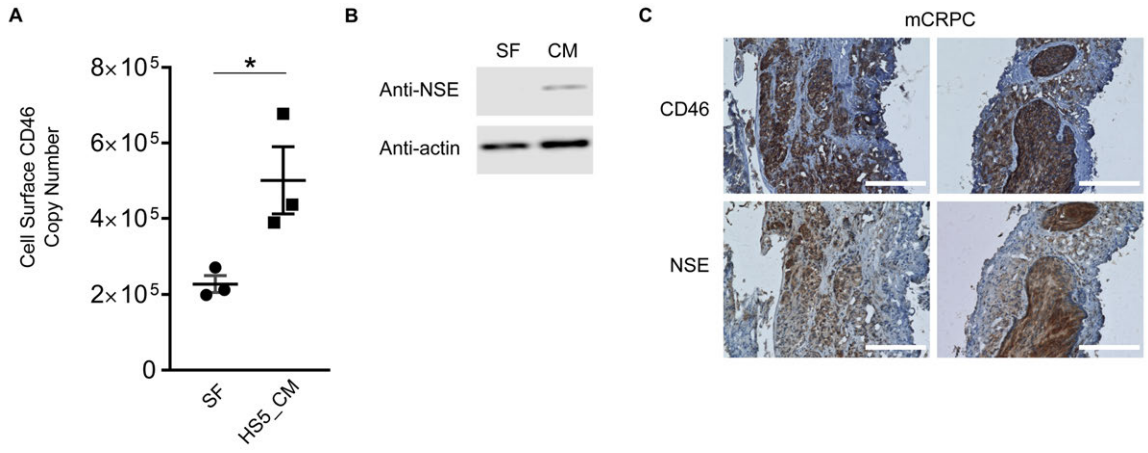

Supplemental Figure S16: Close-up views of CD46 IHC staining (shown in Figure S15C) in neuroendocrine type mCRPC. Scale bar: 150 μm for the left panel, and 30 μm for the right panel (close-up view). For both CD46 and NSE staining, low magnification images in the left panel are from Figure S15, and reshown here to provide the tissue context of high magnification images in the right panel.

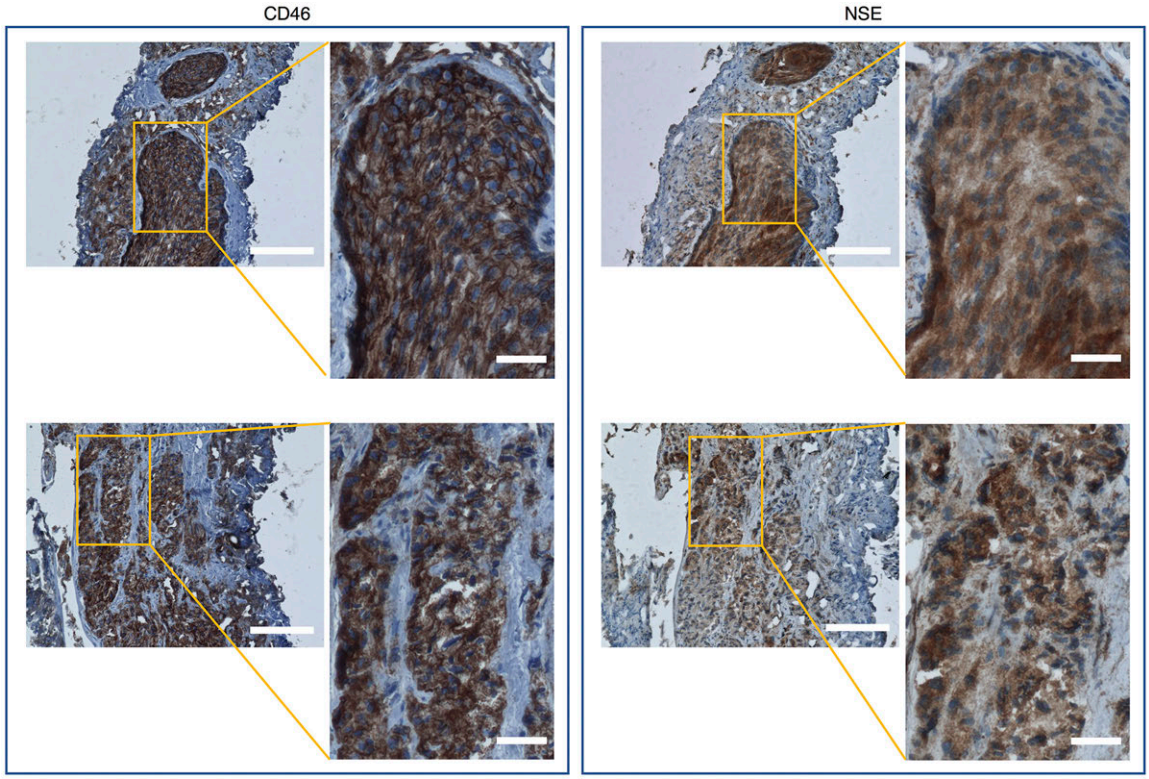

Supplemental Figure S17: CD46 internalization via macropinocytosis by neuroendocrine prostate cancer cell line H660. YS5 IgG1 was incubated with H660 for 24 h and analyzed by confocal microscopy for co-localization with the macropinocytosis marker ND70. The rate of co-localization is 98.82% (84/85). Scale bar: 30 μm.

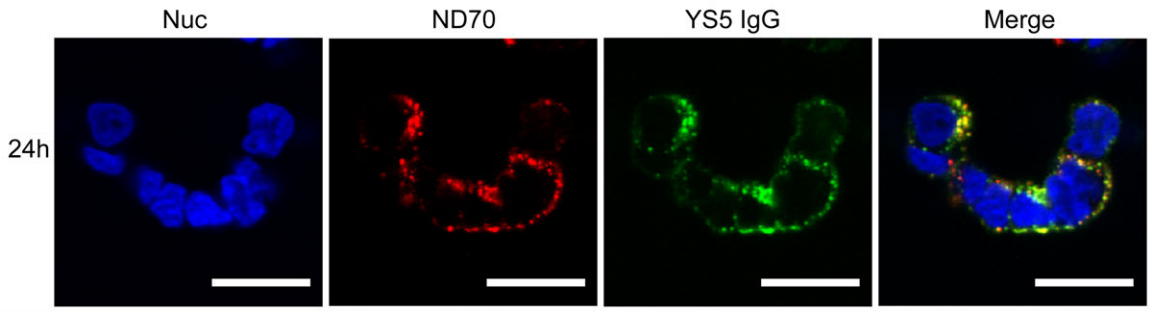

Supplemental Figure S18: Subcellular localization of anti-CD46 antibody post internalization into neuroendocrine prostate cancer cells. YS5 IgG1 was incubated with H660 cells for 4 h and 24 h and analyzed by confocal microscopy. LAMP1 was stained to mark lysosomes. Co-localization between YS5 and LAMP1 was observed at the 4 h time point (10/11 or 90.90%) and increased at the 24 h time point (31/32 or 96.87%). Scale bar: 30 μm.

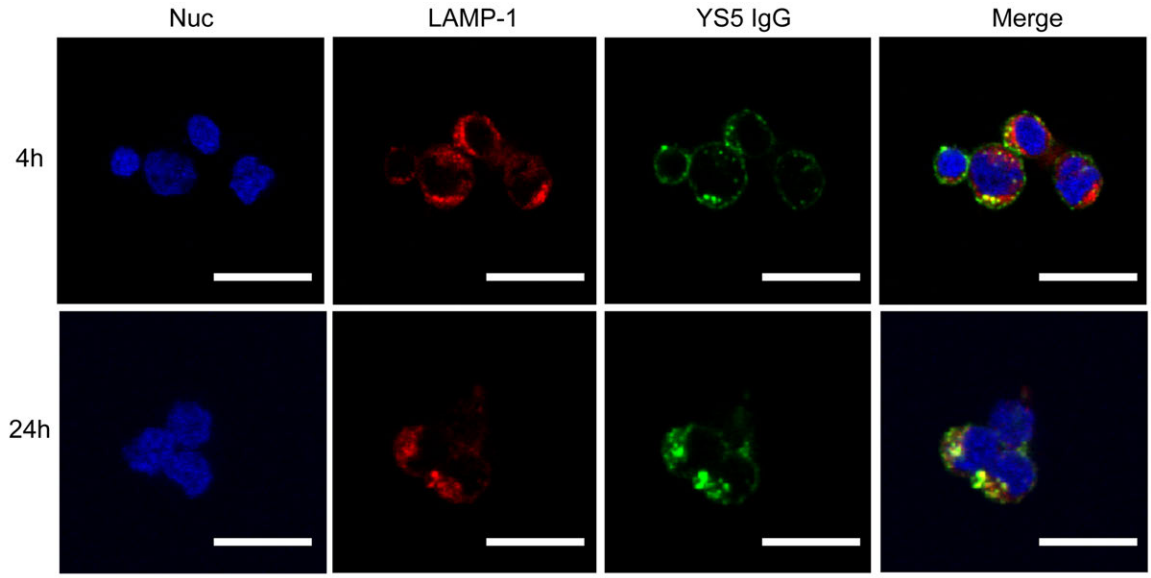

Supplemental Figure S19: CD46 upregulation following ASI treatment. Two mCRPC cell lines DU145 (panel A) and VCaP (panel B) were treated with 5 μM enzalutamide for 7 days. Cell surface CD46 level was measured by FACS using the YS5 antibody. **** $p < 0.0001$. Student's t test, unpaired two-tailed, n = 4.

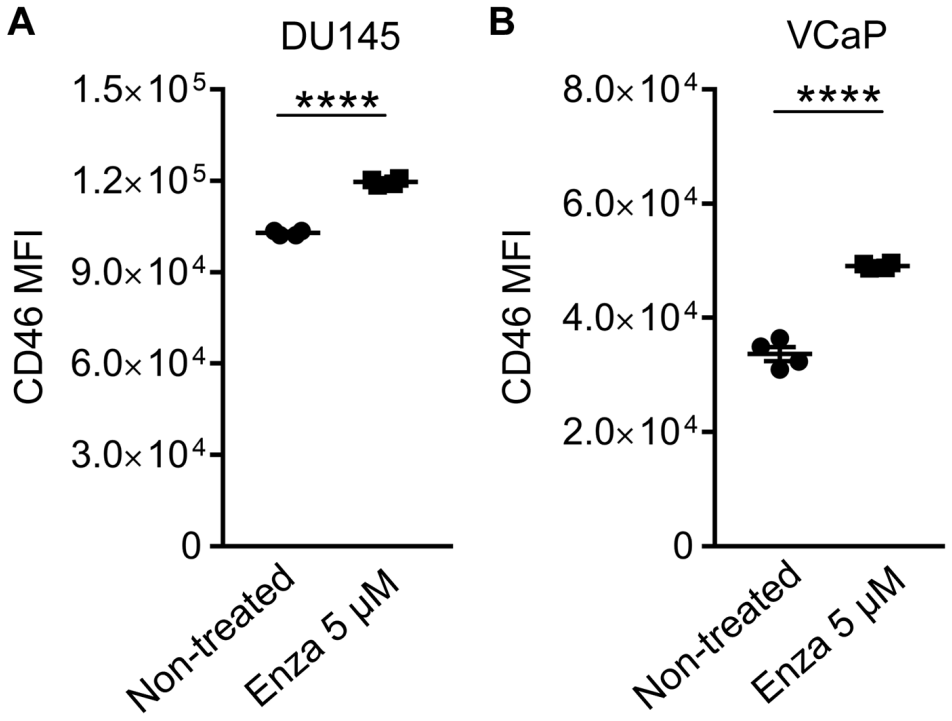

Supplemental Figure S20: Exploratory tox study in non-human primates. Absolute neutrophil counts (ANC) in male (A) and female (B) groups. Two male and two female cynomolgus monkeys for each dosing group (CD46 ADC at 0, 1, and 5 mg/kg), total 12 animals.

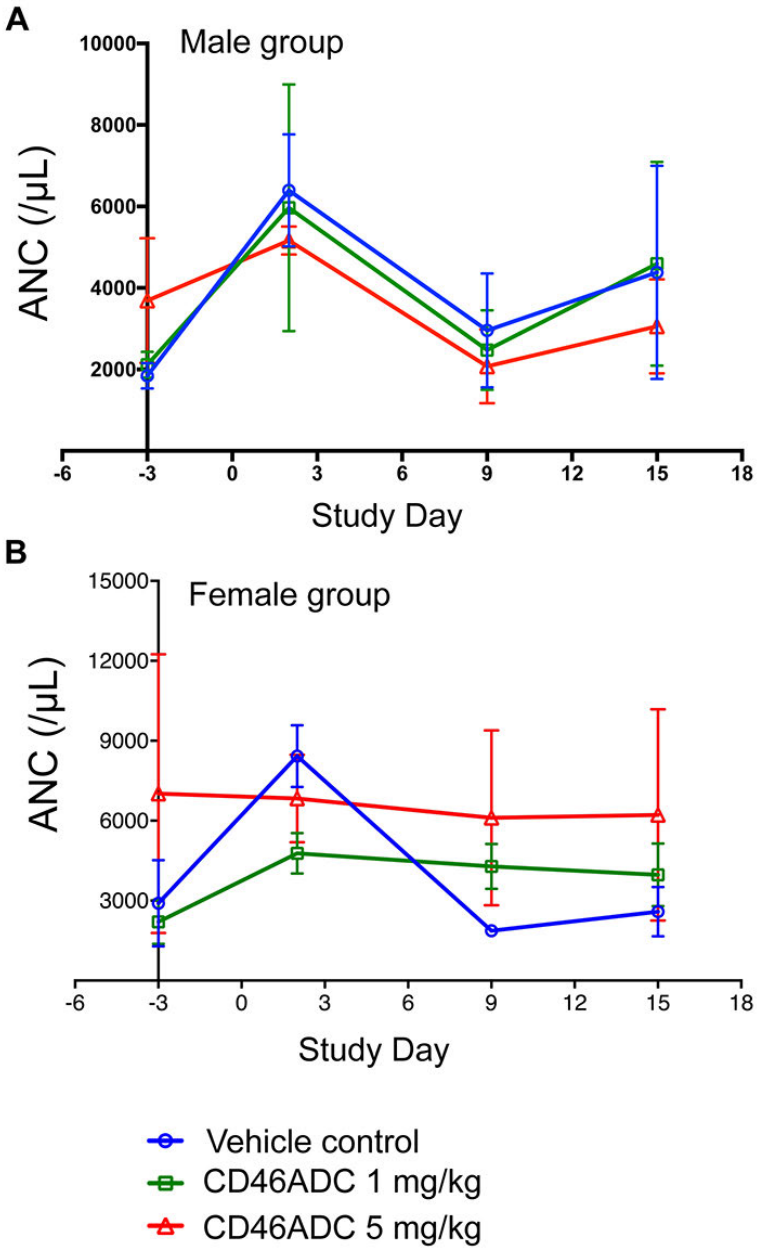

Supplemental Figure S21: Blood chemistry change in exploratory tox study. AST in male (A) and female (B) groups; and ALT in male (C) and female (D) groups. Two male and two female cynomolgus monkeys for each dosing group (CD46 ADC at 0, 1, and 5 mg/kg), total 12 animals.